Directing nanoscale optical flows by coupling photon spin to plasmon extrinsic angular momentum

Y. Lefier, R. Salut, M.A. Suarez, and T. Grosjean*

FEMTO-ST Institute, Université Bourgogne Franche-Comté, UMR CNRS 6174 15B Av. des Montboucons, 25030 Besancon cedex, France

E-mail: thierry.grosjean@univ-fcomte.fr

Abstract

As any physical particle or object, light undergoing a circular trajectory features a constant extrinsic angular momentum. Within strong curvatures, this angular momentum can match the spin momentum of a photon, thus providing the opportunity of a strong spin-orbit interaction. Using this effect, we demonstrate tunable symmetry breaking in the coupling of light into a curved nanoscale plasmonic waveguide. The helicity of the impinging optical wave controls the power distribution between the two counter-propagating subwavelength guided modes, including unidirectional waveguiding. We found experimentally that up to 95 % of the incoupled light can be selectively directed into one of the two propagation directions of a nanoscale waveguide. This approach offers new degrees of freedom in the manipulation of subdiffraction optical modes, and thus appealing new prospects for the development of advanced, deeply subwavelength optical functionalities.

*To whom correspondence should be addressed

Introduction

In addition to its energy, light possesses polarization and spatial degrees of freedom, manifested by its linear momentum as well as spin and orbital angular momenta.[1] Remarkably, spin and orbital momenta are not independent quantities; the spin (circular polarization) can tailor the spatial distribution and propagation direction of light.[2] This phenomenon, known as spin-orbit interaction (SOI), has recently attracted much interest for applications involving light manipulation.[3–11]

Recently, SOI has demonstrated the remarkable property of controlling the directionality of the surface plasmons bound to planar metal-dielectric interfaces.[12–16] The tunability offered by SOI in the directional excitation of planar surface plasmons holds promise of an unprecedented level of control of optical flows in advanced integrated systems and networks. However, planar surface plasmons restrict optical confinement to half the wavelength[17] (despite using subwavelength scale couplers such as metasurfaces or single nanoscale scatterers), and it remains a key challenge to control light propagation directionality in truly nanometer scale plasmonic architectures involving guided modes that are narrowly localized in the vicinity of metal discontinuities.[18–21]

Here, we introduce a new concept of an SOI that enables tunable unidirectional waveguiding at deep subwavelength scale. Such a concept is based on the conversion of the spin angular momentum (SAM) of a diffraction-limited incoming wave to the extrinsic orbital angular momentum (EOAM) of a guided mode within a sharply curved waveguide. It is demonstrated with the helicity-controlled unidirectional coupling of light directly within a bent gap-plasmon waveguide.[22–24] Depending on the sign of their SAM, the incoming photons are shown to couple upstream or downstream within the nanoscale waveguide, with at most 95% of the incoupled energy which is directed towards one of the two propagation directions. This novel SOI is used for distributing photons towards two resonant nano-antennas connected at the ends of the plasmonic transmission line, thus opening new routes in advanced optical functionalities based on truly subwavelength integrated plasmonic circuits.[19,20]

Results and discussions

Our approach relies on the transfer of angular momentum (AM) from an optical wave freely propagating along (0z)-axis, towards a guided mode circulating along a curved trajectory within the perpendicular (xy)-plane (Fig. 1). We focused our attention on the waveguide modes of negligible intrinsic AM. In this case, a curved single-mode waveguide sustains two counter propagating modes whose amplitudes have the azimuthal angular dependence $\exp(\pm i\beta R\phi)$. Here, $\beta = 2\pi/\lambda_{mode}$ is the wave vector and λ_{mode} is the effective wavelength. Analogy with quantum mechanics[25] suggests that such modes are the eigenmodes of the angular momentum operator $L_z = -i\hbar\partial/\partial\phi$, and thus carry extrinsic AM of $\pm\hbar\beta R$ per photon along (0z)($\hbar = h/2\pi$ refers to the Planck constant). The incoupled light being the superposition of these two modes, its EOAM equals $(|a_r|^2 - |a_l|^2)\hbar\beta R$ per photon, where $|a_r|^2$ and $|a_l|^2$ are the probabilities that a guided photon propagates along the two opposite right and left directions, respectively. An impinging plane wave propagating along (0z) carries a SAM of $\sigma\hbar$ per photon oriented along (0z), where σ defines polarization helicity. In the case of an "'elastic"' coupling between the incident photons and a guided mode within an axisymmetrical (circular) waveguide, the longitudinal AM is conserved and the probabilities $|a_r|^2$ and $|a_l|^2$ read:

$$|a_r|^2 = \frac{1+\sigma/\beta R}{2}, \tag{1}$$

$$|a_l|^2 = \frac{1-\sigma/\beta R}{2}. \tag{2}$$

For a linearly polarized incoming wave (σ=0) or a rectilinear waveguide ($R \to \infty$) light coupling is symmetric as $|a_r|^2 = |a_1|^2 = 1/2$. Unidirectionality (ie, $|a_r|^2 = 1$ and $|a_l|^2 = 0$, or vice versa) arises when the SOI satisfies the geometricodynamical condition:

$$\beta = \frac{\sigma}{R}. \tag{3}$$

Equations 1 and 2 thus unveal a trajectory curvature on the subwavelength scale which leads to tunable unidirectional mode coupling. Like in the optical spin hall effect,[3] the SAM-to-EOAM conversion is closely related to a geometric phase, whose gradient is here equal to $\nabla\Phi_G = \sigma/R$. Equation 3 can thus be regarded as the geometric-to-dynamic phase matching originating the unidirectionality.

Equation 3 requires identifying tightly confined guided modes strongly bound to the waveguide, to limit mode leakage in sharply curved trajectories. To fulfill this condition, we focused our attention on the so-called gap-plasmon waveguide design.[22–24] This geometry supports a nanometer scale guided mode whose field distribution is transversely polarized,[23] making it a good candidate for producing the desired geometric phase gradient $\nabla\Phi_G = \sigma/R$.[8] The real conditions also involve an impinging focused beam, rather than a plane wave, and a non axisymmetric lossy waveguide, which may affect the AM conservation introduced above. To further assess surface plasmon directionality in real conditions, we implemented an analytical wave model, based on our SOI-induced geometrical phase Φ_G, to describe the gap plasmon excitation under illumination with a circularly polarized focused beam (see details in the Supporting Information S1.1). Our model shows that under real conditions, unidirectionality is still effective but spectrally shifted with respect to the predictions from Eq. 3 (see Supporting Information S1.2).

We performed full-wave finite-difference time domain simulations (FDTD) of the nanoscale guided mode generated in a bent gap-plasmon waveguide, of 180° curvature angle, patterned on a gold surface. In those simulations, optical waves are focused onto the waveguide curvature under normal incidence with respect to the sample surface, and the mode directionality is studied for various polarizations of the incident beam. The plasmonic structure is designed for operation at $\lambda = 1.55$ μm, corresponding to λ_{mode}=981 nm and an attenuation length $L = 6.67$ μm. The geometrical parameters of the structure are R = 500 nm and $w = 50$nm (gap width), and the thickness of the gold film is 100 nm. The results agree well with our analytical model, in terms of directionality and field distribution within the bent plasmonic waveguide (see Supporting Information S1.2). The slightly lower directionality observed with FDTD simulations (94% with FDTD versus

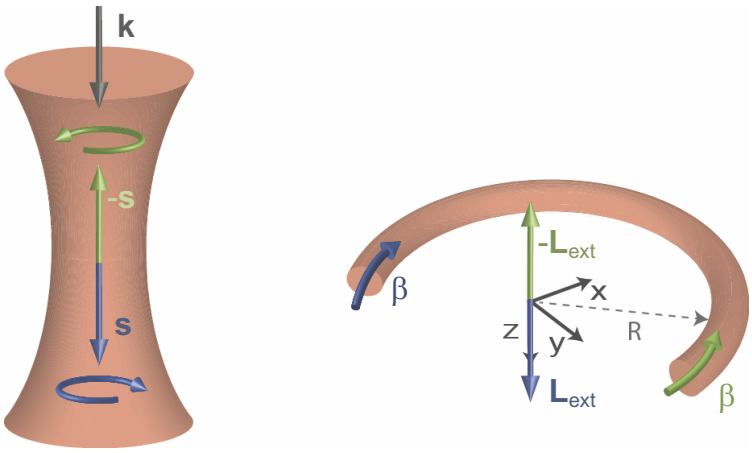

Figure 1: Conditions for SAM-to-EOAM interaction. Longitudinal SAM (**s**) of a freely propagating wave along (0z)-axis together with the EOAM ($\mathbf{L}_{ext}$) of a mode guided along a curved trajectory in the (xy)-plane. Depending on both the polarization handedness of the freely propagating wave and the propagation direction of the guide mode, the SAM and EOAM are parallel or antiparallel. Therefore, if the guided mode is free from intrinsic AM, the SOI between the incident wave and the guided mode is favorable to unidirectional waveguiding. This condition requires a trajectory curvature satisfying $R = \lambda_{mode}/2\pi$ (Eq. 3)

100 % with our model) shows that any residual excitation on both sides of the waveguide bend may lead to a loss of directionality (our model considers excitation only in the waveguide curvature).

We fabricated a curved gap plasmon waveguide of width $w = 50$nm in a 100-nm-thick gold film using focused ion beam milling (FIB)(Fig. 2(a)). On both sides of the curvature, of radius R=500 nm (Fig. 2(b)), the waveguide expands over approximately 5.5 μm (3.54 λ) and the two channels are tilted by 45° after 3 μm to extend the distance between the two waveguide ends to about 2.3 λ. According to our model, such a waveguide curvature reaches tunable directionality at telecommunication wavelengths (Fig. 2(c) and (d)). Two plasmonic coaxial nano-antennas[26] were milled by FIB at the two waveguide ends to impedance match the nanoscale plasmon mode to vacuum and fully control the free-space emission (Fig. 2(e)).[19,20] The inner radius of the coaxial nano-antennas has been set to 150 nm to spectrally center their resonance to 1550 nm. Upon illumination with a linearly polarized light, the emission of an axis-symmetrical coaxial nano-antenna is governed by a transverse electric dipole moment whose orientation is defined by the polarization direction of the incident waves.[26] The near-field coupling between the gap-plasmon waveguide and the coaxial nano-antenna breaks the symmetry degeneracy and leads to a fixed

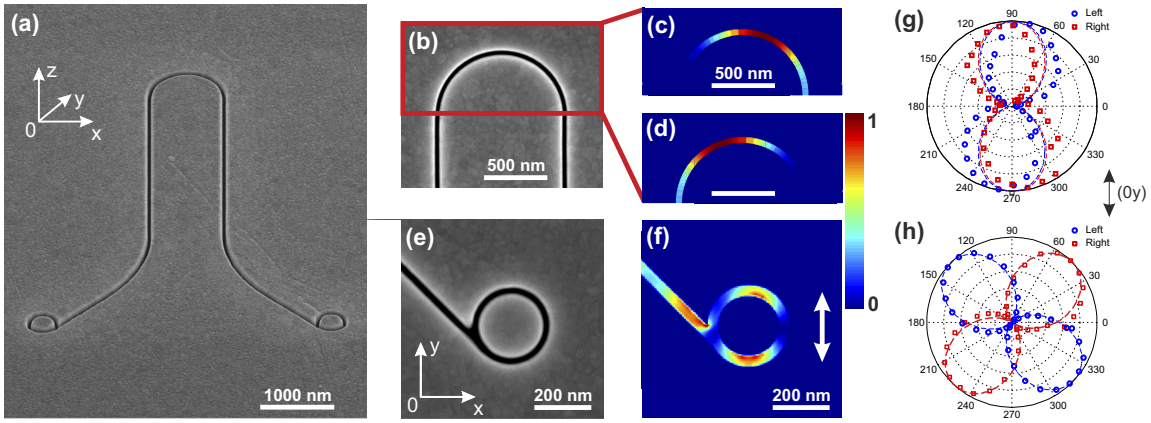

Figure 2: A nanoscale optical transmission-line enabling selective near-field excitation of two resonant coaxial nano-antennas by spin-orbit interaction. (a) Scanning electron micrograph of a subwavelength integrated optical circuit consisting of a bent gap plasmon waveguide connected to coaxial nano-antennas. The structure was fabricated in a gold film for operation at $\lambda = 1.55$ μm. (b) Zoom on the 180° waveguide curvature. (c,d) Simulated electric field intensity within the curved gap-plasmon waveguide under illumination at $\lambda = 1.55$ μm, with our analytical model. The incoming gaussian beam is 1 μm wide, centered to the top of the bend and features (c) circular right and (d) circular left polarization. Our model considered a mode excitation only in the waveguide bend. (e,f) Zoom on the plasmon-fed coaxial nano-antenna: (e) SEM image of the nano-antenna, (f) Simulated electric field intensity within the waveguide and the nano-antenna, with the FDTD method. The nano-antenna shows a dipole moment along the white arrow, ie. parallel to the (0y)-axis. (g) Experimental emission intensity on the left (blue circle) and right (red squares) nano-antennas as a function of the angle θ with respect to (0x)-axis of a linear analyzer placed before the camera. The waveguide bend is excited with a linearly polarized focused beam so that the two nano-antennas are non-radiatively fed by the nanoscale plasmonic waveguide with the same intensity. The results are compared to theoretical predictions (dashed blue and red curves, respectively). (h) Evolution of the experimental emission intensity at the two ends of the same circuit without nano-antennas, in a configuration similar to (g). The infrared camera used for measurements shows a linear response over its entire dynamic range.

emission dipole moment, oriented along the (0y)-axis for both nano-antennas. It is manifested by a two-spot near-field pattern aligned along (0y) (Fig. 2(f)) and a far-field emission linearly polarized along the same direction (see the solid curves of Fig. 2(g)). As a comparison, without nano-antennas, the light emissions at the two waveguide ends are polarized perpendicularly to the waveguide, i.e., orthogonally polarized at 45° of the (0y)-axis (see solid curves of Fig. 2(h)), which is consistent with the polarization properties of the gap surface plasmons.

Directional surface plasmon excitation is carried out with an illumination of the waveguide bend from the front with a circularly polarized beam focused onto the top of the curvature with a $(\times 60, 0.9)$ objective. Part of the incident light is coupled into the waveguide, and thus two counter-propagating plasmonic modes can potentially propagate towards the two nano-antennas ending the nanoscale transmission line. The nano-antennas then efficiently convert the nanoscale surface plasmons into free-space propagating light of controlled polarization, which is detected from the back with a $(\times 125, 0.7)$ objective coupled to a camera. The polarization of the incoming beam is adjusted with a linear polarizer coupled to a quarter-wave plate. Depending on the angle α between the respective element axis, the transmitted field varies from linear ($\alpha = 0°$, 90°) to circular ($\alpha = 45°$, 135°) polarizations, with elliptic polarizations for intermediate angles. First, the optical emission of the two nano-antennas, with an incident linearly polarized focused beam, is analyzed by positioning a rotating linear polarizer before the camera. In accordance with the simulations, the emission intensity of both nano-antennas is maximum when the polarizer is aligned with the (0y)-axis (Fig. 2(g)). Without nano-antennas, the detected signal is, as expected, maximum when the analyzer is aligned across the waveguide (at 45° with respect to (0y)-axis, Fig. 2(h)). The attenuation length of the surface plasmons was measured experimentally to 4.88 ± 1.11 μm by testing structures of different lengths between the waveguide curvature under illumination and the nano-antennas (5.5 μm and 6.5 μm).

The structure is then sandwiched between a circular polarizer ($\alpha = 45°$ or 135°) and a linear analyzer (Fig. 3(a)). Figs. 3(b) and (c) show the images of the structure for the right and left-handed circular polarizations of the incident beam, respectively. Each image shows two light spots: the

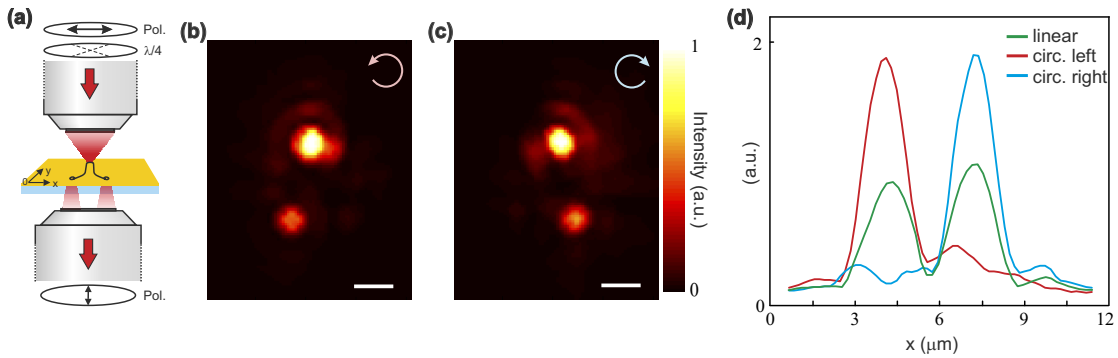

Figure 3: Spin-orbit interaction directs surface plasmons on the nanometer scale. (a) Schematic diagram of the optical set-up used for characterizing the surface plasmon directionality within our nanoscale network. (b,c) Optical emission from the structure observed with (b) left circular and (c) right circular polarizations. The state of incident polarization is shown by red and blue arrows, respectively. (d): intensity profile across the two nano-antennas with left circular (red curve), right circular (blue curve) and linear (green curve) excitation polarization. The linear polarization is parallel to the (0x)-axis.

brighter spot of fixed position is the excitation spot at the waveguide bend whereas the other one, whose position changes from Fig. 3(b) to Fig. 3(c), corresponds to the emission of a single nano-antenna non-radiatively fed with the nanoscale surface plasmons. The observed far-field emissions (Figs. 3(b) and (c)) agree well with the surface plasmon directionality theoretically predicted with our analytical model (Fig. 2(c) and (d), respectively). Circularly polarized light beams of opposite handedness generate localized optical emission at either the right or the left coaxial nano-antenna whereas linearly polarized light induces hot spots of equal intensity profiles at both nano-antennas (Fig. 3(d)). Importantly, the emission intensity obtained with linearly polarized incident light is half the emission intensity reached in circular polarization (Fig. 3(d): the overall power emitted by the two nano-antennas with linearly polarized light is transferred to a single nano-antenna with circular polarization. This property confirms that the nano-antenna near-field addressing undergoes SOI. The coupling directionality was estimated from the relative nano-antenna emission intensities deduced from Figs. 3(b) and (c). In accordance with FDTD simulations, the directionality for both circular polarizations is equal to 95 %.

The emission intensities of the nano-antennas are shown in Fig. 4 as a function of the polarization of the incident light. The polarization is set by the angle α between the polarizer and the

quarter wavelength plate in the illumination system. These results agree well with the polarization-dependent distribution of incoming photons in the spin states "right" and "left", whose respective intensities $|\psi_r|^2$ and $|\psi_l|^2$ read:

$$|\psi_r|^2 = \frac{1}{2}(1+\sin 2\alpha), \quad (4)$$

$$|\psi_l|^2 = \frac{1}{2}(1-\sin 2\alpha), \quad (5)$$

the helicity of the incoming beam being defined as $\sigma = |\psi_r|^2 - |\psi_l|^2 = \sin 2\alpha$. For all angles α, the incident photons prepared in the right and left spin states are selectively directed to the nano-antennas on the right and left, respectively, leading to a directional coupling tunable with polarization. Such a tunability confirms that the non-radiative excitation process of the two nano-antennas undergoes an SOI process. Therefore, the helicity of the incident waves is capable of tuning the energy shared between the two branches of a transmission line that remotely addresses two nano-antennas in an ultracompact architecture.

The excitation efficiency of the gap surface plasmons has been numerically predicted to be 2.54% at λ=1.55 μm (see Supporting Information S1.3). As shown in this study, such a coupling appears to be high enough to develop advanced functionalities under far-field monitoring with an objective and a standard camera. It could however be enhanced by implementing couplers based on resonant nano-antennas.[27] In that case, we could expect longer and more complex plasmonic networks.

Conclusion

In conclusion, we introduced and demonstrated the concept of an SOI based on the transfer of the SAM of light to the EOAM of surface plasmons confined and guided in a nanometer-scale metallic waveguide. Such a concept enabled helicity-controlled tunable addressing of two resonant

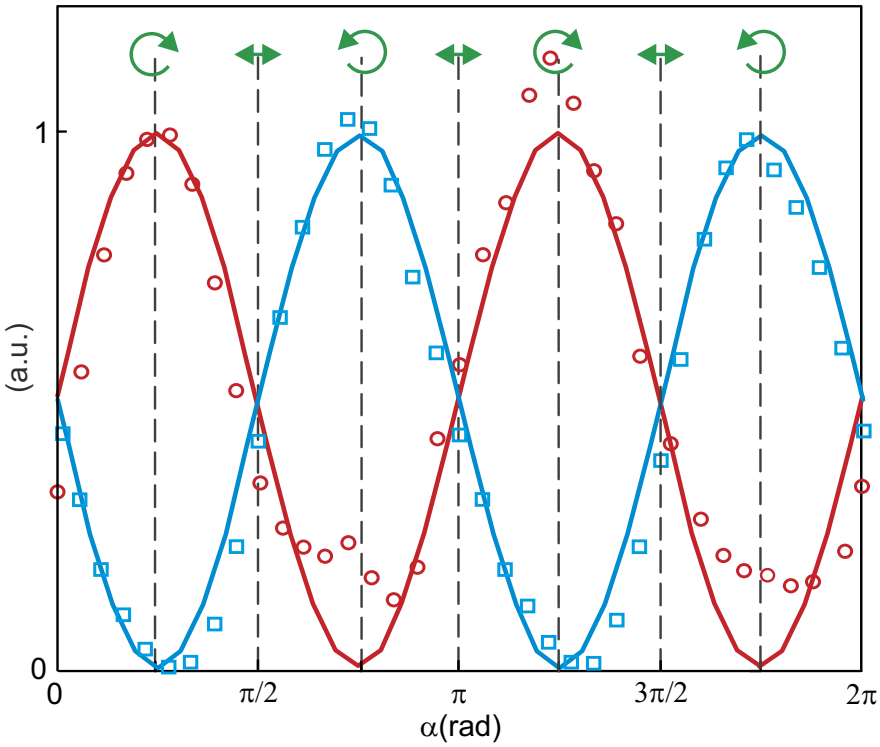

Figure 4: Changing the incident polarization enables continuous tuning of the directionality of the launched nanoscale guided mode. Evolution of the emission intensities of the two fabricated nano-antennas as a function of the polarization of the incoming beam. The incident polarization is set by the angle α between a polarizer and a quarter wavelength plate in the illumination system. It varies continuously from linear state (α =0, $\pi/2$) to left and right circular states ($\alpha = \pi/4$ and $3\pi/4$, respectively) with intermediate elliptic states.

nano-antennas connected at the two ends of a nanoscale gap-plasmon waveguide. Our approach opens new perspectives in manipulating deeply subwavelength optical fields within ultra-compact systems made of interconnected nano-optical elements. More generally, SOI within nanoscale devices has the potential of becoming a key building block of future nano-optical technologies.

Acknowledgement

The authors are indebted to Ulrich Fischer for helpful discussions, and to Cara Leopold for her support. This work is supported by the Labex ACTION program (contract ANR-11-LABX-01-01), and by the French RENATECH network and its FEMTO-ST technological facility.

Notes

The authors declare no competing financial interest.

Supporting Information Available

- S1.1. Analytical model: description of the analytical model for assessing nanoscale surface plasmon directionality in real conditions,
- S1.2. Unidirectionality with an incident focused beam: study with our analytical model of the mode directionality within the curvature of a gap-plasmon waveguide, under illumination with a circularly polarized focused beam.
- S1.3. Excitation efficiency of the gap surface plasmons.

This material is available free of charge via the Internet at `http://pubs.acs.org/`.

References

(1) Allen, L.; Beijersbergen, M. W.; Spreeuw, R.; Woerdman, J. *Phys. Rev. A* **1992**, *45*, 8185.

(2) Bliokh, K.; Rodríguez-Fortuño, F.; Nori, F.; Zayats, A. *Nat. Photonics* **2015**, *9*, 796–808.

(3) Bliokh, K. Y.; Bliokh, Y. P. *Phys. Rev. Lett.* **2006**, *96*, 073903.

(4) Petersen, J.; Volz, J.; Rauschenbeutel, A. *Science* **2014**, *346*, 67.

(5) Rodriguez-Herrera, O. G.; Lara, D.; Bliokh, K. Y.; Ostrovskaya, E. A.; Dainty, C. *Phys. Rev. Lett.* **2010**, *104*, 253601.

(6) Bomzon, Z.; Kleiner, V.; Hasman, E. *Opt. Lett.* **2001**, *26*, 1424–1426.

(7) Shitrit, N.; Bretner, I.; Gorodetski, Y.; Kleiner, V.; Hasman, E. *Nano Lett.* **2011**, *11*, 2038–2042.

(8) Bliokh, K. Y.; Gorodetski, Y.; Kleiner, V.; Hasman, E. *Phys. Rev. Lett.* **2008**, *101*, 030404.

(9) Brasselet, E.; Gervinskas, G.; Seniutinas, G.; Juodkazis, S. *Phys. Rev. Lett.* **2013**, *111*, 193901.

(10) Gorodetski, Y.; Drezet, A.; Genet, C.; Ebbesen, T. W. *Phys. Rev. Lett.* **2013**, *110*, 203906.

(11) Le Feber, B.; Rotenberg, N.; Kuipers, L. *Nat. Commun.* **2015**, *6*.

(12) Lin, J.; Mueller, J. B.; Wang, Q.; Yuan, G.; Antoniou, N.; Yuan, X.-C.; Capasso, F. *Science* **2013**, *340*, 331–334.

(13) Xi, Z.; Lu, Y.; Yu, W.; Wang, P.; Ming, H. *J. Optics* **2014**, *16*, 105002.

(14) Rodriguez-Fortuno, F. J.; Marino, G.; Ginzburg, P.; OConnor, D.; Martinez, A.; Wurtz, G. A.; Zayats, A. V. *Science* **2013**, *340*, 328–330.

(15) Mueller, J. B.; Leosson, K.; Capasso, F. *Nano Lett.* **2014**, *14*, 5524–5527.

(16) Shitrit, N.; Yulevich, I.; Maguid, E.; Ozeri, D.; Veksler, D.; Kleiner, V.; Hasman, E. *Science* **2013**, *340*, 724–726.

(17) Novotny, L.; Hecht, B. *Principle of nano-optics*; Cambridge University Press, 2006.

(18) Gramotnev, D. K.; Bozhevolnyi, S. I. *Nat. Photonics* **2010**, *4*, 83–91.

(19) Huang, J.-S.; Feichtner, T.; Biagioni, P.; Hecht, B. *Nano Lett.* **2009**, *9*, 1897–1902.

(20) Kriesch, A.; Burgos, S. P.; Ploss, D.; Pfeifer, H.; Atwater, H. A.; Peschel, U. *Nano Lett.* **2013**, *13*, 4539–4545.

(21) Lefier, Y.; Grosjean, T. *Opt. lett.* **2015**, *40*, 2890–2893.

(22) Pile, D. F.; Ogawa, T.; Gramotnev, D. K.; Matsuzaki, Y.; Vernon, K. C.; Yamaguchi, K.; Okamoto, T.; Haraguchi, M.; Fukui, M. *Appl. Phys. Lett.* **2005**, *87*, 261114.

(23) Veronis, G.; Fan, S. *Opt. Lett.* **2005**, *30*, 3359.

(24) Liu, L.; Han, Z.; He, S. *Opt. Express* **2005**, *13*, 6645–6650.

(25) Marcuse, D. *Light transmission optics*; Van Nostrand Reinhold New York, 1972.

(26) Baida, F. I.; Belkhir, A.; Van Labeke, D.; Lamrous, O. *Phys. Rev. B* **2006**, *74*, 205419.

(27) Andryieuski, A.; Zenin, V. A.; Malureanu, R.; Volkov, V. S.; Bozhevolnyi, S. I.; Lavrinenko, A. V. *Nano lett.* **2014**, *14*, 3925–3929.

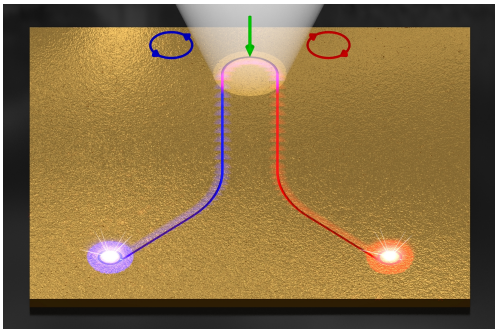

Figure 5: For TOC only